Current **A**pplied **S**cience and **T**echnology e-ISSN: 2586-9396

Curr. Appl. Sci. Technol. ….., Vol... (No...), e0268380

Research article

Tailoring Structural, Optical, and Electrical Properties of ITO Thin Films via Thickness Control, Reactive Nitrogen, and Thermal Annealing

Pathomporn Junbang[1], Montri Aiempanakit[2], Chantan Aiempanakit[3] and Kamon Aiempanakit[4]*

[1]Department of Physics, Faculty of Medicine, Bangkok Thonburi University, Thawi Watthana, Bangkok, 10170, Thailand
[2]Department of Physics, Faculty of Science, Silpakorn University, Nakhon Pathom, 73000, Thailand
[3]Division of Physics, Faculty of Science and Technology, Rajamangala University of Technology Thanyaburi, Pathumthani, 12110, Thailand
[4]Department of Physics, Faculty of Science and Technology, Thammasat University, Pathumthani, 12121, Thailand

Received: 14 July 2025, Revised: 9 October 2025, Accepted: 9 November 2025, Published: 17 February 2026

Abstract

In this study, indium tin oxide (ITO) and nitrogen-incorporated ITO (ITON) thin films with thicknesses of 57, 116, and 173 nm were deposited on glass substrates using DC magnetron sputtering. The effects of nitrogen incorporation, film thickness, and thermal annealing on the structural, optical, and electrical properties were investigated. X-ray diffraction (XRD) analysis revealed that ITON exhibited partial crystallization in the as-deposited state and influenced the preferred crystal orientation after annealing, with ITO favoring (400) and ITON favoring (222). Both materials demonstrated high optical transparency (>70%) in the visible range, with ITON exhibiting higher transmittance, particularly at thickness of 173 nm (84.79% after annealing). The optical bandgap decreased with increasing thickness but increased after annealing, with ITON maintaining consistently higher values. Electrical measures indicated a thickness-dependent resistivity trend. Un-annealed ITO showed a systematic sheet resistance decrease from 546.4 to 255.83 Ω/square, whereas annealed ITO exhibited a minimum sheet resistance of 208.5 Ω/square at 173 nm. ITON films initially displayed unmeasurable sheet resistance at lower thicknesses, but after annealing, sheet resistance decreased systematically from 1789.0 to 447.23 Ω/square. Despite the low nitrogen concentration (0.01%), its incorporation significantly influenced the structural and electrical properties of the films. These findings provide insights into optimizing ITON thin films for advanced optoelectronic applications.

Keywords: ITO thin films; DC magnetron sputtering; thickness effect; optical and electrical properties; structural characterization

*Corresponding author: E-mail: akamon@tu.ac.th
https://doi.org/10.55003/cast.2026.268380

1. Introduction

Indium tin oxide (ITO) is one of the most widely used transparent conducting oxide (TCO) materials, with extensive applications in flat-panel displays, touch screen panels, light-emitting diodes, solar cells, and electrochromic devices (also known as "smart windows") (Granqvist, 2007; Ellmer, 2012). To meet the growing demand for high-performance ITO films, various deposition techniques have been developed, including chemical vapor deposition, electron beam evaporation (Nuchuay et al., 2017), sol-gel processing (Biswas et al., 2015), spray pyrolysis (Zhang et al., 2017), pulsed-laser deposition (Atabaev et al., 2017), and magnetron sputtering—both direct current (DC) (Kim et al., 2018; Huang et al., 2024; Markov et al., 2023) and radio frequency (RF) (Kurdesau et al., 2006; Robb et al., 2024). Among these, magnetron sputtering remains the most attractive technique, as it enables the production of high-quality thin films with excellent uniformity and scalability for industrial applications.

The properties of ITO films deposited by magnetron sputtering depend on several parameters, including substrate temperature (Jung & Lee, 2003), target composition (Jung & Lee, 2003; Qiao & Mergel, 2005), working gas pressure, oxygen flow during reactive deposition (Hao et al., 2008; Kim et al., 2009; Das et al., 2007), and film thickness (Pokaipisit et al., 2007; Hao et al., 2008; Amalathas & Alkaisi, 2016). While ITO films are often deposited at elevated temperatures (Kurdesau et al., 2006; Kim et al., 2018) or subjected to post-deposition annealing (Antony et al., 2004) to enhance their optical and electrical properties, some applications require low-temperature processing. This includes deposition on temperature-sensitive substrates, such as polymers and semiconductor thin films, where thermal annealing may induce undesirable property changes (Hotovy et al., 2013; Markov et al., 2023; Huang et al., 2024). The high optical transmittance of ITO films is primarily attributed to their wide bandgap (3.5-4.6 eV) semiconductor nature (Fan & Goodenough, 1977; Balasubramanian & Subrahmanyam, 1989). The fundamental absorption edge lies in the ultraviolet (UV) region and exhibits a blue shift with increasing carrier concentration, following the Burstein–Moss effect (Gupta et al., 1989). Various strategies have been explored to enhance the electrical and optical properties of ITO, depending on specific technological requirements. These include compositional modifications such as replacing ITO with zinc–indium–tin oxide (Phillips et al., 1995; Minami et al., 1998) and implanting H_2^+ or O^+ ions to modify defect states (Shigesato et al., 1993). However, early investigations on ITO films produced by DC magnetron sputtering in different plasma environments, including nitrogen (N_2)-containing gases, remain limited (Fraser & Cook, 1972). Incorporating nitrogen into ITO has been reported to provide several advantages compared with conventional ITO. Nitrogen can effectively passivate oxygen vacancies and suppress excessive free carrier concentration, thereby reducing free carrier absorption and enhancing optical transmittance in the visible range (Shigesato et al., 1993; Aperathitis et al., 2003). Additionally, nitrogen incorporation can optimize carrier density, thereby improving electrical conductivity without significantly compromising transparency (Avelar-Muñoz et al., 2020). It also enhances oxidation resistance and chemical stability under high-temperature conditions, leading to improved film durability (Aiempanakit et al., 2009; Kim et al., 2009). Furthermore, nitrogen incorporation can modify the band structure, resulting in a slight widening of the optical bandgap through the reduction of defect states, while simultaneously improving film stability and microstructural uniformity (Cho & Kim, 2013; Nguyen et al., 2020). These improvements directly address key limitations of conventional ITO films, such as high free carrier absorption, defect-induced scattering, and instability under elevated processing temperatures. Despite these

potential benefits, systematic studies on the influence of nitrogen incorporation, particularly in films with thicknesses below 200 nm, remain scarce. To date, there has been no comprehensive study on indium–tin–oxynitride (ITON) thin films, particularly in relation to thickness-dependent properties. ITO films are typically deposited with thicknesses in the range of several hundred nanometers (Gorjanc et al., 2002; Kurdesau et al., 2006; Das et al., 2007; Hao et al., 2008; Eshaghi & Graeli, 2014; Amalathas & Alkaisi, 2016). However, recent studies have investigated thicker films (1–3 μm) for specialized applications, such as light–matter interactions (Ni et al., 2020) and protective coatings for mirrors (Atabaev et al., 2017). Furthermore, nanocomposite hard coatings have been synthesized using magnetron sputtering (Polychronopoulou et al., 2008), arc evaporation (Polychronopoulou et al., 2009), and electron beam evaporation (Rebholz et al., 2007). Despite these advancements, there have been few studies on the influence of thicknesses below 200 nm, particularly when nitrogen incorporation is involved.

To address this gap, we investigated the effects of nitrogen incorporation on ITO thin films prepared by DC magnetron sputtering, focusing on three thicknesses (57, 116, and 173 nm). We systematically examined the structural, electrical, and optical properties of these films before and after thermal annealing, providing new insights into how nitrogen modifies film characteristics at the nanoscale.

2. Materials and Methods

ITO and ITON films were prepared by DC magnetron sputtering on glass substrates at room temperature using an ITO target (99.99% purity, 2 inches in diameter and 0.25 inches thick) composed of 90 wt% In_2O_3 and 10 wt% SnO_2. The glass substrates were ultrasonically cleaned in acetone, methyl alcohol, and deionized water before deposition. The DC sputtering process was carried out in a reactive atmosphere using two different working gases: Ar only for ITO and $Ar+N_2$ for ITON. The flow rate of working gases was maintained at 15 sccm for all depositions. The distance between the ITO target and the glass substrate was 8.0 cm, and the DC power was kept constant at 20 W.

A rotary pump and diffusion pump system achieved a base pressure of 5×10^{-5} mbar before introducing working gases. The working pressure during ITO film deposition for Ar gas was 2.8×10^{-3} mbar, while that for ITON was 1.8×10^{-2} mbar. We prepared films with thicknesses ranging from 57 to 173 nm under different working gas conditions. The sputtering deposition parameters for ITO and ITON samples are listed in Table 1. After deposition, the films were annealed in air at 500°C for 1 h to investigate the effects of thermal treatment on structural, electrical, and optical properties.

Film characterization included morphological analysis using field emission scanning electron microscopy (FE-SEM, Tescan/Mira3, Czech Republic) for surface and cross-sectional imaging. The crystalline structure was studied by X-ray diffraction (XRD, Bruker, D2 Phaser) in the range of 20°-80° with the Cu Kα emission line (λ = 1.54056 Å). Optical properties were measured using ultraviolet-visible spectroscopy (G10S UV-vis, Thermo Scientific) in the 300-1000 nm wavelength range. The average optical transmittance (%T) in the visible region (380-780 nm) was calculated using a weighted average method to account for the human eye's spectral sensitivity. The calculation followed the standard photopic luminous efficiency function, where the relative spectral energy $E(\lambda)$ represents the normalized intensity distribution of visible light, such that the sum of $E(\lambda)$ over the visible range equals 100. The average transmittance was determined using equation (1):

$$\%T = \frac{\sum_{\lambda_a}^{\lambda_b} T(\lambda)E(\lambda)}{\sum_{\lambda_a}^{\lambda_b} E(\lambda)} \quad (1)$$

where *T(λ)* is the spectral transmittance at wavelength λ, and *E(λ)* is the relative energy at that wavelength, defined as *E(λ) = [(Energy(λ) × 100) / Total Energy].* This method ensures that the calculated %T accurately reflects the photometric response of the human eye, allowing a realistic comparison of film transparency in the visible range. Sheet resistance (R_s) was determined using the four-point probe method.

Table 1. Sputtering deposition parameters of ITO and ITON samples

Fixed Parameters	**Range**					
Target	In_2O_3 (90wt%)/SiO_2 (10wt%)					
Substrate	Glass					
Working pressure	$5x10^{-2}$ mbar					
DC power	20 W					
ITO, Ar flow rate (sccm)	15					
ITON, Ar+N_2 flow rate (sccm)	15 + 15					
Varies parameters	**Types of films**					
	ITO			**ITON**		
Deposition rate (nm/sec)	0.28			0.14		
Deposition time(sec)	203	410	614	400	800	1200
Thickness (nm)	57±2.22	116±3.62	173±6.27	57±2.46	116±4.85	173±3.16
FWHM (deg)	3.58	2.66	2.15	1.92	1.51	1.02
Crystalline size (222) (nm)	2.35	3.16	3.92	3.43	4.11	5.14
FWHM at annealed films 500°C (deg)	2.45	2.05	1.63	1.32	1.12	0.81
Crystalline size (222) at annealed films 500°C (nm)	4.38	5.56	6.95	6.35	7.49	10.3

3. Results and Discussion

3.1 Structural properties

The structural evolution of the ITO and ITON thin films with varying thicknesses (57, 116, and 173 nm) was investigated using XRD before and after thermal annealing at 500°C for 1 h, as shown in Figures 1(a)-(d). The as-deposited ITO films exhibited broad diffraction peaks centered at approximately 2θ = 30.64°, characteristic of an amorphous or poorly crystallized structure (Figure 1(a)). This amorphous nature was consistent across all film thicknesses, indicating that the initial structural disorder was independent of the film

thickness, which has already been reported several times by other authors (Hu et al., 2004; Wang & Tang, 2017; Mazur et al., 2022). In contrast, the as-deposited ITON thin films displayed a distinct crystalline peak corresponding to the (222) plane at 2θ ≈ 30.64°, according to JCPDS no. 01-089-4596, superimposed on a broad amorphous background (Figure 1(c)). The presence of this crystalline peak suggests that nitrogen incorporation promotes partial crystallization, even at room temperature (Gartner et al., 2014).

Thermal annealing in air at 500°C for 1 h induced significant structural transformations in both film types. The ITO films exhibit well-defined diffraction peaks corresponding to the cubic In_2O_3 structure (Figure 1(b)). The observed diffraction patterns revealed multiple crystallographic planes: (211), (222), (400), (411), (431), (440), (611), and (622) at 2θ values of approximately 21.8°, 30.64°, 35.70°, 37.88°, 45.81°, 51.18°, 56.4°, and 61°, respectively. The (400) orientation is the preferred growth direction (Aiempanakit et al., 2009; Ollotu et al., 2020; Amrani et al., 2023). The annealed ITON films similarly demonstrated crystallization into the cubic In2O3 structure (Figure 1(d)) but with notably different preferential orientations. The (222) peak dominated the diffraction pattern. This distinction suggests that nitrogen incorporation fundamentally affects the crystal growth direction, possibly owing to modified interfacial energetics or growth kinetics. Both ITO and ITON thin films showed improved crystallinity with increasing thickness, as evidenced by decreasing FWHM values of the (222) peak while maintaining consistent peak positions across all thickness, indicating thickness-dependent crystal growth but a thickness-independent crystal structure (Hukari et al., 2002; Liu et al., 2021).

The degree of crystallinity was quantitatively assessed using the Scherrer equation (2), where the crystallite size (D) was calculated from the FWHM of the (222) diffraction peak with application of a shape factor of 0.92.

$$D = \frac{0.92\lambda}{FWHM\ \cos\theta} \tag{2}$$

Where λ is the X-ray wavelength and FWHM is the full width at half maximum, calculated from the (222) plane shown in Figures 1(a)-(d). As illustrated in Figure 2(a), the crystalline size exhibited a clear increasing trend with film thickness. The 57 nm film exhibited broadest diffraction peak (largest FWHM), corresponding to the smallest crystalline size and lowest crystallinity. Conversely, the 173 nm film exhibited the narrowest peak (smallest FWHM), corresponding to the largest crystallite size and highest crystallinity. The variation of FWHM values with thickness is explicitly shown in Figure 2(b). The as-deposited ITO films possess the lowest crystalline size, ranging from 2.35-3.92 nm, whereas the as-deposited ITON films show higher values across all thicknesses, ranging from 3.43-5.14 nm. This indicates that nitrogen promotes partial crystallization during the film deposition stage, without requiring additional thermal treatment.

Upon annealing at 500°C for 1 h, both ITO and ITON films exhibited reduced FWHM values, reflecting enhanced crystallinity and significant grain growth. At a thickness of 173 nm, the annealed ITO film's crystalline size grew to 6.95 nm, while the annealed ITON film at the same thickness achieved a maximum crystalline size of 10.3 nm. This demonstrates that N_2 not only accelerates initial crystallization but also effectively promotes subsequent crystal growth when combined with thermal treatment.

The contrasting crystallization behavior between the ITO and ITON thin films can be attributed to the role of N_2 in the crystal structure (Yang et al., 2020). While thermal annealing promoted crystal growth through increased atomic mobility and lattice reorganization in both cases, N_2 incorporation appeared to facilitate initial nucleation even before thermal treatment.

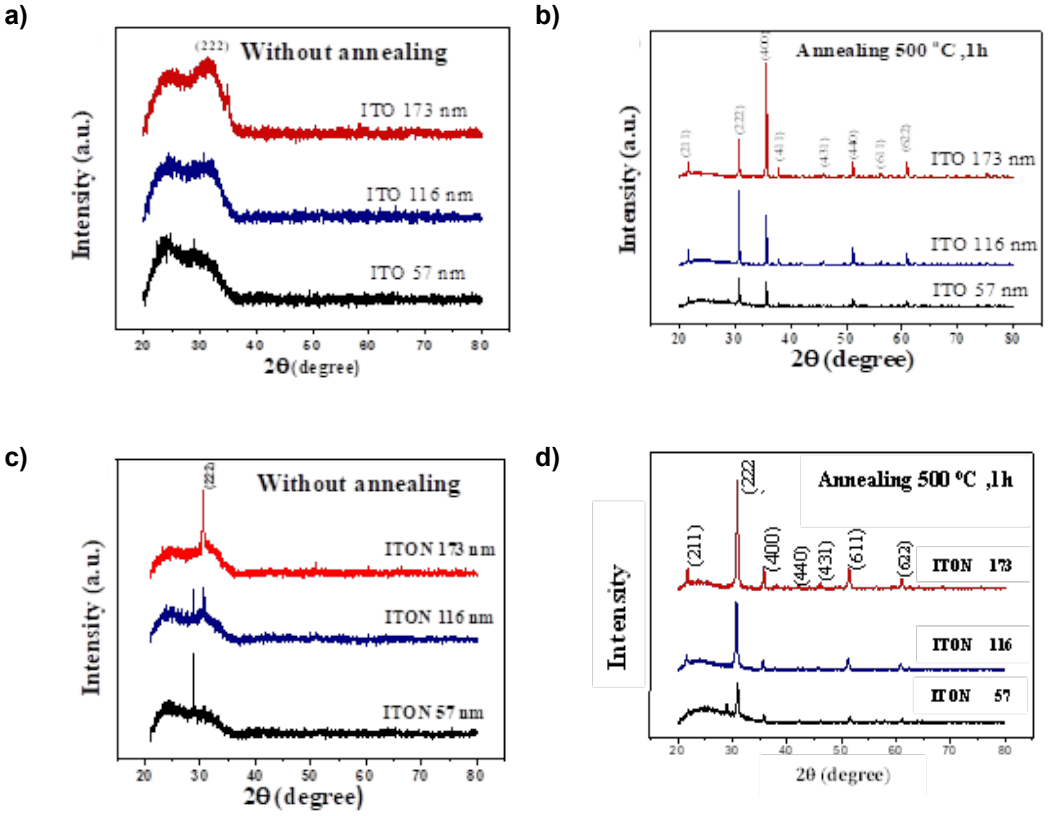

Figure 1. X-ray diffraction patterns for ITO and ITON films without annealing and annealing at a temperature of 500°C for 1h

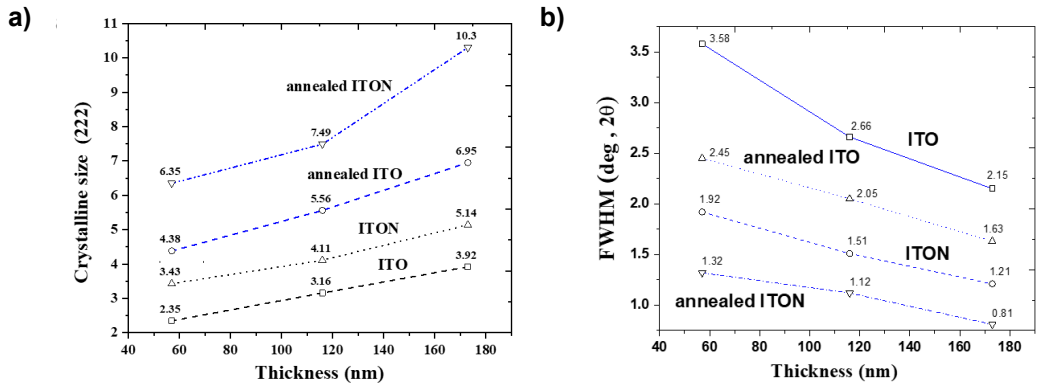

Figure 2. Crystalline size a) and FWHM b) of ITO and ITON films without annealing and annealing at a temperature of 500°C for 1h

However, the presence of N_2 also influences the final crystal structure, particularly the preferred orientation and overall crystal system. The persistence of the preferred (222) orientation in ITON thin films through the annealing process suggests that N_2 plays a crucial role in determining the energetically favorable growth direction of the crystal structure (Liu et al., 2021).

FE-SEM was employed to investigate the surface morphologies of the ITO and ITON films before and after thermal annealing at 500°C for 1 h, as shown in Figure 3. Cross-sectional FE-SEM images were obtained to confirm the film thicknesses of the ITO and ITON samples. For the ITO films (Figures 3(a)-(c)), the measured thicknesses were 57 nm, 116 nm, and 173 nm, respectively. Similarly, comparable thicknesses were achieved for the ITON films (Figures 3(d)-(f)), allowing for direct comparison between the two film types.

The as-deposited ITO films exhibited relatively smooth surfaces with subtle texture variations. The 57 nm films showed a uniform, largely featureless surface characteristic of amorphous structures. As the thickness increased to 116 and 173 nm, the films maintained similar smooth characteristics with only marginally increased surface roughness, suggesting uniform growth conditions during deposition. This morphological uniformity correlates well with the XRD results, indicating an amorphous structure in the as-deposited state (Lacroix et al., 2022). In contrast, the as-deposited ITON films displayed distinct surface features even before thermal treatment. The 57 nm film revealed subtle granular features, while the 116 nm films showed visible, uniformly distributed nanoscale grains across the surface. The 173 nm films maintained a similar granular texture, though slightly less pronounced than the intermediate thickness. This inherent granular morphology aligns with the XRD observations of partial crystallization in the as-deposited ITON films, as evidenced by the presence of the (222) peak (Chen et al., 2019).

Thermal annealing induced significant morphological changes in both film types. The annealed ITO thin films developed progressive crystallization features with increasing thickness. The 57 nm films showed a fine granular texture with small, uniformly distributed crystallites. The 116 nm and 173 nm films exhibited increasingly pronounced granular structures while maintaining a uniform distribution across the surface. This gradual enhancement in the crystalline character corresponds to the decreased FWHM values observed with increasing film thickness (Figure 2(b)). The annealed ITON thin films displayed a more complex morphological evolution (Ollotu et al., 2020). The 57 nm films showed a fine granular texture with uniformly distributed small crystallites. Most notably, the 116 nm films exhibited distinct void-like features or cavities scattered across the surface, along with crystalline grains. The 173 nm films, however, returned to a more uniform and smoother surface with a finer grain structure and absence of voids (Ollotu et al., 2020).

3.2 Elemental composition

Energy dispersive X-ray (EDX) spectroscopy was employed to analyze the elemental compositions of the ITO and ITON thin films. The EDX spectra shown in Figure 4 confirm the presence of indium (In), tin (Sn), and oxygen (O) in all samples, while nitrogen (N) was detected only in the ITON films. The quantitative elemental composition data are summarized in Table 2, demonstrating systematic variations with film thickness. Notably, the nitrogen concentration in ITON films was measured at approximately 0.01 at.%, despite the use of an $Ar:N_2$ (50:50) working gas mixture.

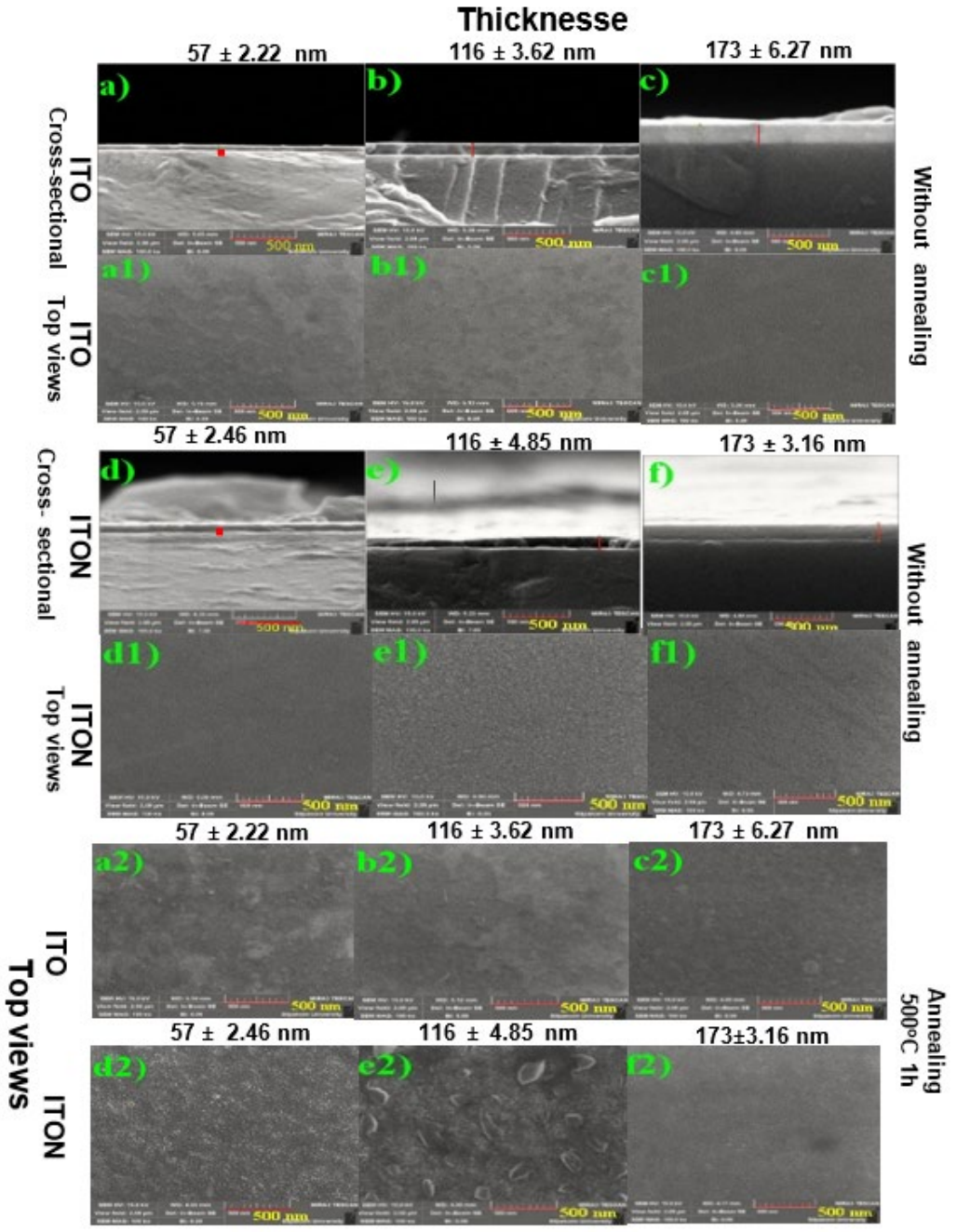

Figure 3. Cross-sectional SEM images of the (a-c) ITO (d-f) ITON films and Top views (a1-c1) ITO (d1-f1) ITON without annealing and top views (a2-c2) ITO (d2-f2) ITON after annealing 500°C1h

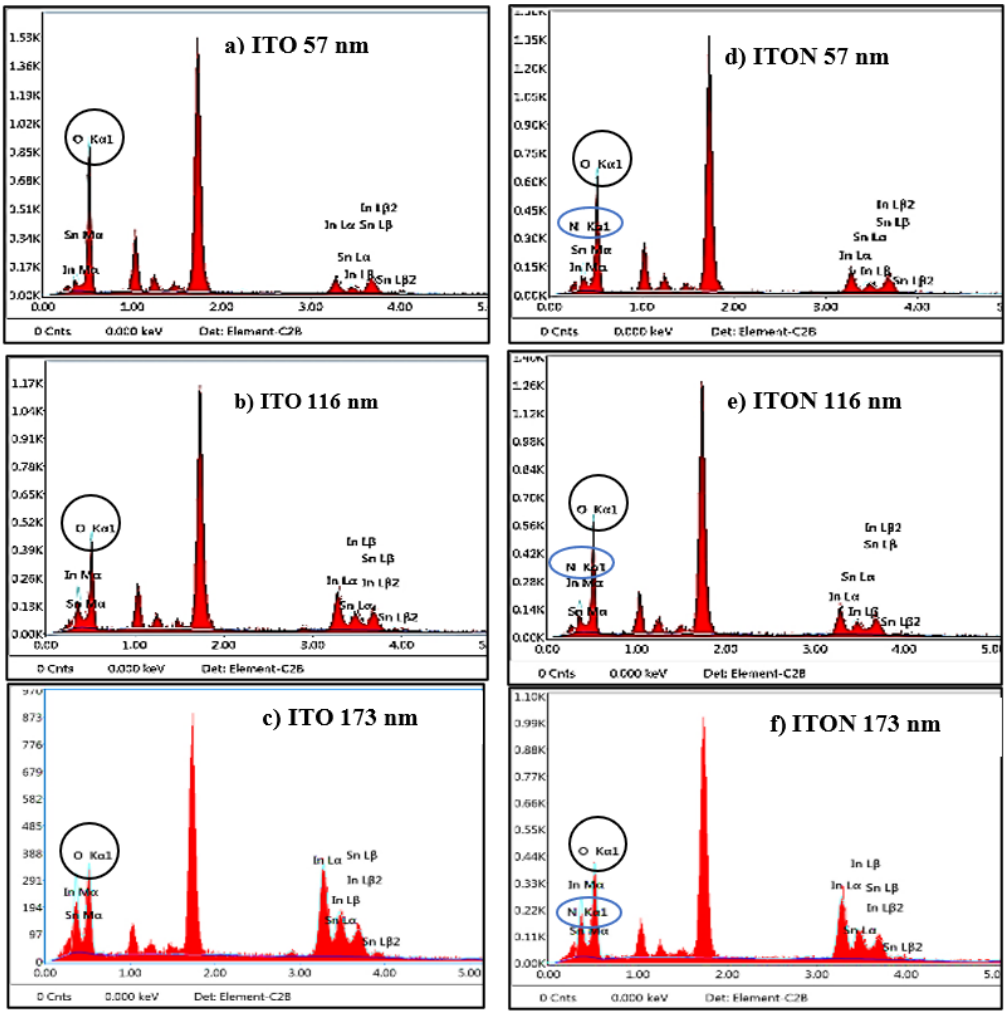

Figure 4. EDX measurement of (a, b, c) ITO and (d, e, f) ITON films on glass substrates at different film thicknesses

Table 2. The elemental composition of ITO and ITON films at different thickness values

Sample	EDX				
	In/at.%	Sn/at.%	O/at.%	N/at.%	Sn/In
ITO (57 nm)	4.07	1.37	94.56	-	0.34
ITON (57 nm)	6.14	1.58	92.27	0.01	0.26
ITO (116 nm)	10.22	2.91	86.87	-	0.28
ITON (116 nm)	7.27	2.27	90.44	0.01	0.31
ITO (173 nm)	17.83	3.77	78.40	-	0.21
ITON (173 nm)	13.65	2.96	83.38	0.01	0.21

This low nitrogen content can be rationalized by the mechanism of nitrogen incorporation during sputtering. The dissociation energy of the N≡N bond (9.8 eV) is much higher than that of O_2 (5.1 eV), resulting in limited ionization efficiency of N_2 under plasma conditions. Consequently, nitrogen atoms have a lower probability of substituting oxygen in the ITO lattice and are more likely to occupy grain boundary or interstitial sites rather than form stable substitutional bonds (Yang et al., 2019).

Comparison with previous reports indicates that such low nitrogen incorporation is consistent with literature values under similar deposition conditions. For example, Yang et al. (2019) reported nitrogen levels below 0.05 at.% in ITON films deposited by DC magnetron sputtering using Ar/N_2 gas mixtures. Similarly, Tchenka et al. (2021) and Liu et al. (2023) demonstrated that even at high N_2 flow ratios, nitrogen incorporation remained limited, highlighting the intrinsic difficulty of introducing significant nitrogen into the ITO lattice by sputtering.

In addition, nitrogen loss mechanisms must be considered. During deposition, energetic Ar^+ bombardment can induce re-sputtering of weakly bonded nitrogen species from the growing film surface. Furthermore, incorporated nitrogen may be unstable during post-deposition oxidation, where oxygen from residual gases in the chamber or from ambient exposure preferentially replaces nitrogen at shallow binding sites (Aperathitis et al., 2003; Hu et al., 2004). These effects, combined with the limited sensitivity of EDX to light elements, contribute to the very low measured nitrogen concentrations.

Despite its trace concentration, nitrogen incorporation is confirmed by both the detection of N Kα signals in the EDX spectra (Figures 4(d)-(f)) and by the structural modifications observed in XRD, where ITON films exhibit distinct (222) diffraction peaks that are not present in ITO films of similar thickness (Figure 1(c)). This indicates that even minimal nitrogen incorporation can influence crystallization behavior and optical transmittance, consistent with previous findings on ITON systems (Yang et al., 2019; Tchenka et al., 2021).

3.3 Optical properties

The optical characteristics of the ITO and ITON thin films were investigated using UV–visible–NIR spectroscopy for three different thicknesses (57, 116, and 173 nm), both before and after thermal annealing at 500°C. The optical transmittance spectra were measured in the wavelength range of 300-1100 nm, as shown in Figures 5(a)-(b). All samples exhibited high optical transparency in the visible spectrum (400-800 nm), with transmittance values exceeding 70%. The results demonstrated clear dependencies on both film thickness and annealing conditions.

For ITO films, thermal annealing significantly improved optical performance at all thicknesses. The most pronounced enhancement was observed in the 57 nm film, where annealing increased the maximum transmittance from approximately 75% to 80%. Although the effect of annealing became less prominent with increasing film thickness, both 116 nm and 173 nm ITO films still exhibited noticeable improvement, maintaining good transparency throughout the visible range (Li et al., 2023). This observation emphasizes the role of thickness in governing optical properties, particularly in thinner films. Specifically, the 57 nm film showed the highest increase in transmittance following annealing, while the 116 nm and 173 nm films displayed slightly lower increases but remained stable, consistent with previous findings (Koseoglu et al., 2015).

In the case of ITON films, thermal annealing yielded varied effects depending on thickness. For 57 nm and 116 nm films, annealing resulted in modest increases in

transmittance. However, the as-deposited 173 nm ITON film showed a unique behavior, with a pronounced transmittance peak of approximately 90% around 500 nm. After annealing, this peak shifted slightly, and the transmittance gradually decreased at longer wavelengths in the NIR region (800-1100 nm). Each film's thickness exhibited distinct optical features, highlighting the strong influence of N_2 incorporation, especially at higher thicknesses. In the NIR region, annealed 57 nm and 116 nm ITON films maintained stable transmittance (~85%), while the 173 nm sample showed a decreasing trend down to ~70% (Gartner et al., 2014).

Figure 5(c) presents the transmittance (%T) in the visible range (380-370 nm), calculated using the weighted average method described in Section 2. For ITO, the average transmittance increased from 75.60% (57 nm) to 81.19% (116 nm), remaining nearly constant at 173 nm. Annealing further improved these values across all thicknesses, yielding 77.34% (57 nm), 81.40% (116 nm), and 82.11% (173 nm) (Aperathitis et al., 2003; Nguyen et al., 2020). ITON films exhibited even higher initial transmittance values than ITO films, beginning at 79.59% (57 nm), increasing to 81.27% (116 nm), and reaching 82.97% (173 nm). After annealing, these values rose further to 81.00%, 81.18%, and 84.79%, respectively. The highest transmittance value observed in this study was for the annealed 173 nm ITON film at 84.79% (Aperathitis et al., 2003).

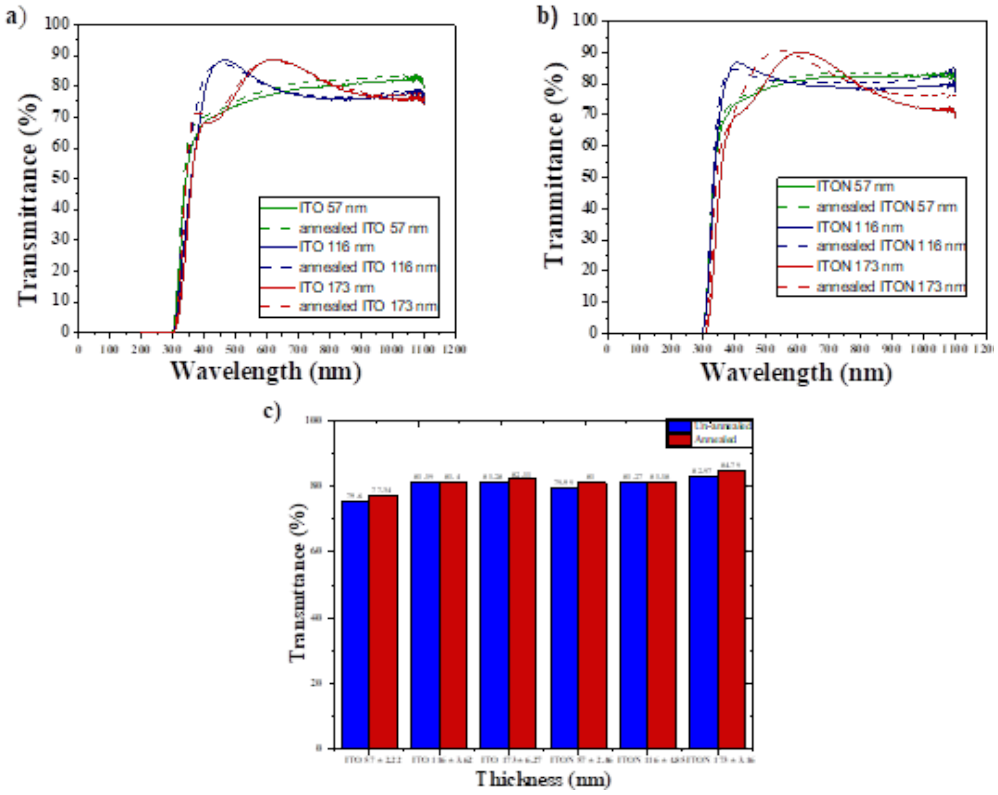

Figure 5. Optical transmittance of ITO and ITON thin films. (a) ITO films before and after annealing. (b) ITON films before and after annealing. (c) transmittance (%) (400-800 nm) of ITO and ITON films

These trends can be explained by multiple interrelated mechanisms. Increased transmittance with film thickness is attributed to improved crystallinity in thicker films. A greater material volume enables better crystal growth and alignment, reducing light scattering at grain boundaries and defects. Thermal annealing at 500°C enhances these effects through several structural improvements: transformation of amorphous regions into crystalline domains (as supported by FWHM-based XRD analysis.), grain coalescence, reduction in boundary density, and improved atomic organization. These improvements contribute to minimizing scattering and optical absorption (Aiempanakit et al., 2009). Furthermore, the higher transmittance consistently observed in ITON films correlates with their higher sheet resistance. This relationship implies the significant of lower free carrier concentrations, which reduce absorption via intraband transitions, consistent with previous observations in nitrogen-incorporated ITO systems (Aperathitis et al., 2003). Together, these findings illustrate the synergistic roles of film thickness, N_2 incorporation, and annealing in tuning the optical transparency of ITO-based thin film.

3.4 Energy gap analysis

The E_g values of the ITO and ITON thin films were investigated as a function of film thickness and thermal treatment. Figure 8 shows the E_g values plotted against film thickness for the deposited and annealed films. For as-deposited ITO films, the E_g values decrease with increasing thickness: 4.04 eV at 57 nm, 4.00 eV at 116 nm, and 3.92 eV at 173 nm. After annealing at 500°C, a slight increase in E_g values was observed across all thicknesses: 4.05 eV at 57 nm, 4.01 eV at 116 nm, and 3.94 eV at 173 nm, as shown in Figures 6(a)-(f). ITON films exhibited consistently higher E_g than their ITO counterparts did. The as-deposited ITON films showed E_g of 4.06 eV at 57 nm, 4.03 eV at 116 nm, and 3.95 eV at 173 nm. Annealing further increased these values to 4.08 eV, 4.05 eV, and 3.98 eV for 57 nm, 116 nm, and 173 nm films, respectively, as shown in Figures 7(g)-(l). The decrease in the E_g with increasing film thickness correlates with the increase in absorbance observed in thicker films (Lai et al., 2023). As film thickness increases, the free carrier absorption increases, leading to a higher carrier concentration in thicker films (Thakur et al., 2007). The relationship between thickness and carrier concentration influences the E_g of the material. The consistently higher E_g values observed in the ITON films suggest that N_2 incorporation modifies the absorption characteristics of the material (Wang et al., 2022). The increase in the E_g values after thermal treatment for both ITO and ITON thin films indicates that annealing influences the optical properties of the material as it improves crystallinity and reduces structural defects, as confirmed by FWHM-based XRD analysis (Koseoglu et al., 2015). The highest E_g (4.08 eV) was observed in the annealed ITON at 57 nm. In contrast, the lowest E_g (3.92 eV) was found in the as-deposited ITO at 173 nm, demonstrating the significant impact of both N_2 incorporation and thermal treatment on the optical properties of these films (Fallah et al., 2007). This consistently higher E_g in ITON films supports the conclusion from previous work that N_2 incorporation induces a fundamental change in the material's band structure, an effect that cannot be explained by carrier concentration changes alone (Aperathitis et al., 2003).

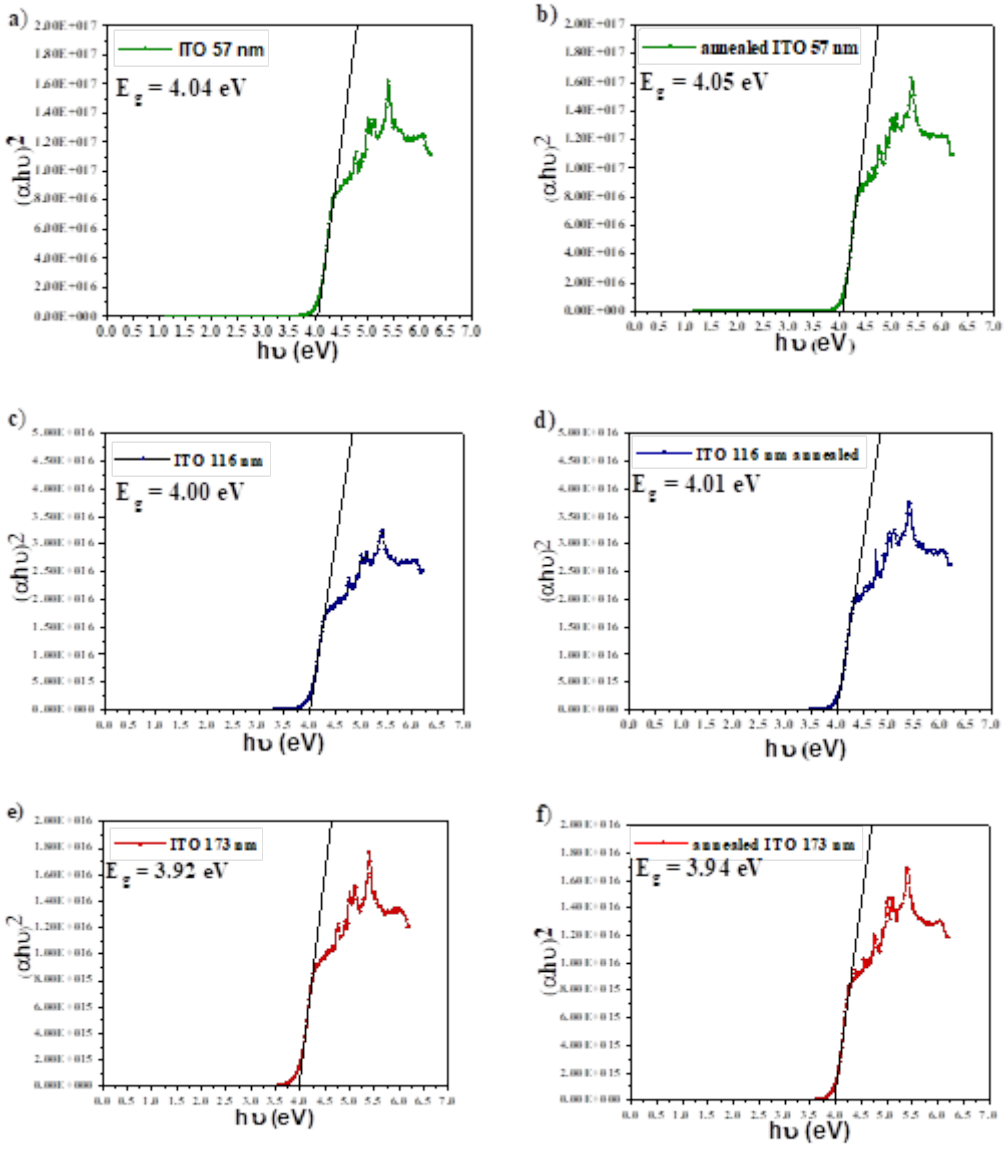

Figure 6. Tauc plot for E_g determination of ITO films: (a, c, e) as-deposited films and (b, d, f) after annealing at 500°C for 1 h

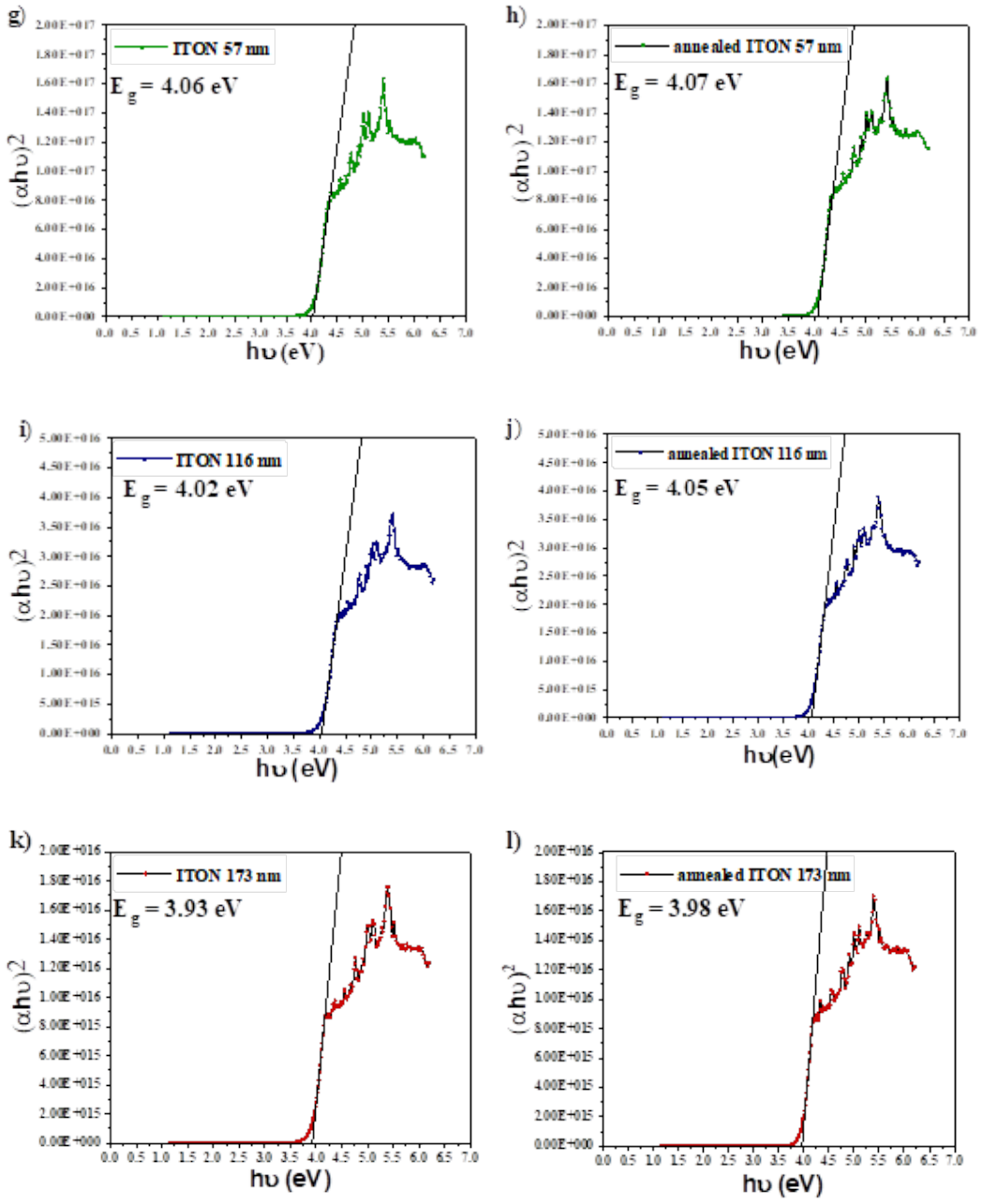

Figure 7. Tauc plot for E_g determination of ITON films: (g, i, k) as-deposited films and (h, j, l) after annealing at 500°C for 1 h

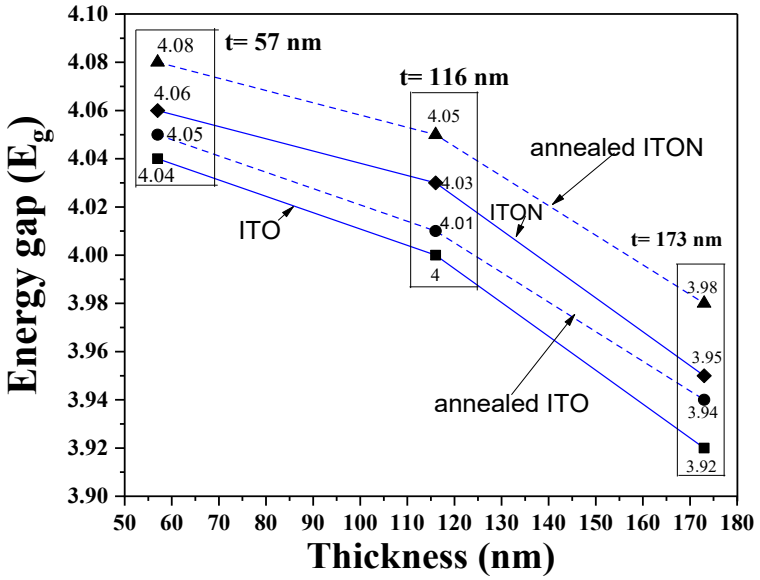

Figure 8. Variation in optical band gap values of ITO and ITON films before and after annealing at 500°C for 1 h

3.5 Electrical properties

In Table 3, the electrical properties of the ITO films demonstrate distinct thickness-dependent behaviors in both the as-deposited and annealed states. The sheet resistance for the as-deposited ITO films shows a consistent decreasing trend with increasing thickness (546.4 → 307.8 → 255.83 Ω/square). This behavior can be attributed to the improved carrier mobility in thicker films due to better crystallinity and fewer grain boundaries, coupled with reduced surface and interface scattering effects (Li et al., 2023). Upon thermal annealing at 500°C, the films exhibit more complex behavior, with sheet resistance showing non-monotonic thickness dependence (765.33 → 2093.67 → 208.5 Ω/square) (Pokaipisit et al., 2008). This relationship between the film thickness, crystallinity, and sheet resistance reveals an interesting interplay between the structural factors. At 57 nm, despite showing lower crystallinity in the XRD patterns, the film maintained a relatively smooth, continuous structure with fewer structural defects and grain boundaries (Zubair et al., 2019). While less crystalline, this morphology provided relatively unimpeded pathways for electron transport, resulting in a moderate sheet resistance of 765.33 Ω/square. The 116 nm film, despite exhibiting higher crystallinity as evidenced by more substantial XRD peaks, develops a more disrupted crystal structure during the annealing process. The increased thickness provides sufficient material for crystallization but results in incomplete structural development, leading to numerous grain boundaries and defects. These structural imperfections act as electron scattering sites, significantly impeding carrier transport and resulting in a markedly higher sheet resistance (2093.67 Ω/square) (Zubair et al., 2019).

Table 3. Sheet resistance values of ITO and ITON films at different thicknesses in as-deposited and annealed states

Sample	Sheet resistance (Ω/square)	
	as-deposited	annealed
ITO-commercial	32.42	57.77
ITO (57nm)	546.40	765.33
ITO (116 nm)	307.80	2093.67
ITO (173 nm)	255.83	208.50
ITON (57 nm)	No detect	1789.0
ITON (116 nm)	No detect	649.96
ITON (173 nm)	765.60	447.23

In contrast, the 173 nm film provides sufficient material volume to develop complete and stable crystal structures, as evidenced by the most substantial XRD peaks. This more complete crystallization results in a well-ordered structure with optimized grain boundaries, facilitating efficient electron transport and yielding the lowest sheet resistance (208.5 Ω/square) among the three thicknesses studied. This thickness-dependent behavior demonstrates that the quality and completeness of the crystal structure formation, rather than merely the degree of crystallinity, play a crucial role in determining the electrical properties of ITO films.

The electrical behavior of the ITON films showed distinct characteristics in the as-deposited and annealed states. For un-annealed ITON films, resistivity measurements at 57 nm and 116 nm were undetectable, becoming measurable only at 173 nm (765.6 Ω/square), aligning with the thickness-dependent structural effects previously reported in the literature. Sparvoli et al. (2013) demonstrated that indium oxynitride film thickness significantly influences resistivity through structural and electrical property changes. According to their findings, thinner films exhibit substantially higher resistivity owing to increased grain boundary scattering and potential defects, which in our case likely exceeded the measurement limits of the four-point probe method. As the thickness increased to 173 nm, a sufficient material volume allowed for improved crystallinity and reduced boundary effects, resulting in measurable conductivity. This thickness-dependent behavior is particularly pronounced in the N_2-incorporated films compared with the pure ITO, highlighting how N_2 modification of the film structure amplifies these thickness-related effects. Upon annealing, the ITON films demonstrated a clear correlation between crystalline and electrical properties. The XRD patterns show a progressive enhancement in crystallinity with increasing thickness, from the weakest diffraction peak at 57 nm to the strongest, well-defined peak at 173 nm. This structural evolution directly corresponds to the observed resistivity trend: the 57 nm film, with the lowest crystallinity, exhibited the highest sheet resistance (1789.0 Ω/square) because of its more disordered structure, which created numerous barriers for electron transport. The 116 nm films showed intermediate crystallinity and sheet resistance (649.96 Ω/square), reflecting improved structural order and thus better electron mobility. The 173 nm film displayed the highest degree of crystallinity with sharp, well-defined diffraction peaks. It achieved the lowest sheet resistance (447.23 Ω/square) because its well-ordered crystal structure provides optimal pathways for electron conduction with minimal scattering. This relationship between the structural order and electrical properties illustrates how enhanced crystallinity reduces the number of electron scattering sites and facilitates more efficient charge transport in N_2-incorporated ITO films. This higher resistivity in N_2-incorporated films can be attributed to the occupation of oxygen vacancies by N atoms, which reduces the free

carrier concentration and consequently impedes electron transport (Aperathitis et al., 2003). From EDX analysis, the N atomic percentage (N/at.%) in ITON films remains consistently at 0.01% across all thicknesses, which aligns with observations reported in the paper of Avelar- Muñoz et al. (2020), where the N_2 incorporation in such films typically maintains values lower than 1%. Despite these trace amounts, N_2 incorporation substantially influences both the structural and electrical characteristics of the films, as evidenced by the distinct XRD patterns and resistivity behaviors discussed previously.

4. Conclusions

ITO and ITON thin films with thicknesses of 57 nm, 116 nm, and 173 nm were successfully deposited using DC magnetron sputtering and characterized before and after thermal annealing at 500°C for 1 h. Despite its low concentration (0.01%), incorporated N_2 significantly influenced the structural, optical, and electrical properties of films. Structural analysis revealed that N_2 promotes partial crystallization even in as-deposited ITON films, whereas ITO remains purely amorphous before annealing. After thermal treatment, both materials exhibited enhanced crystallinity with increasing thickness, but different preferred orientations were developed (400) for ITO and (222) for ITON. This indicates that N_2 incorporation fundamentally alters crystal growth dynamics. Optical analysis showed that both materials maintained high transmittance (>70%) in the visible range, with ITON films consistently exhibiting higher transmittance than ITO. The annealed 173 nm ITON film achieved the highest transmittance of 84.79%, highlighting N's role in modifying the optical properties. Bandgap analysis confirmed a consistent thickness dependence, where both ITO and ITON exhibited lower E_g with increasing thickness, but values increased overall after annealing. ITON maintained higher E_g than ITO across all conditions. The electrical analysis demonstrated distinct thickness-dependent resistance behaviors. Un-annealed ITO exhibited a systematic resistance reduction with increasing thickness, while annealed ITO showed non-monotonic behavior, achieving the lowest sheet resistance of 208.5 Ω/square at 173 nm. ITON films initially exhibited unmeasurable resistivity at lower thicknesses, but after annealing, sheet resistance decreased progressively with the thickness (1789.0 → 447.23 Ω/square). This confirms a direct correlation between crystallinity and sheet resistance, where higher crystallinity leads to improved conductivity. These findings highlight the significant impact of N_2 incorporation on ITO thin film properties, even at trace concentrations. Additionally, they demonstrate how film thickness, N_2 incorporation, and thermal treatment collectively influence crystallinity, optical behavior, and electrical performance, providing valuable insights for optimizing ITO-based optoelectronic materials.

5. Acknowledgements

This research was supported by the Science Fund for Research and Innovation of Thailand, Fiscal Year 2024, Thammasat University and by funding from the Research and Academic Services Group, Bangkok Thonburi University. The authors sincerely thank these organizations for their financial support and encouragement throughout this study.

6. Authors' Contributions

Pathomporn Jufigures andbuted to the conceptualization and methodology of the study, conducted the investigation and experimental work, performed the formal analysis,

prepared the figures, and drafted the original manuscript. Montri Aiempanakit provided supervision, contributed to experimental design guidance, assisted with data interpretation, and participated in writing—review and editing. Chantan Aiempanakit contributed to technical consultation, supported validation of the experimental data, and assisted in writing—review and editing. Kamon Aiempanakit supervised the overall project, provided essential resources and scientific guidance, and contributed to writing—review and editing.

ORCID

Pathomporn Junbang https://orcid.org/0009-0006-3865-0596

7. Conflicts of Interest

The authors declare no conflicts of interest.

References

Aiempanakit, K., Rakwamsuk, P., & Dumrongrattana, S. (2009). Influence of continuous and discontinuous depositions on properties of ITO films prepared by DC magnetron sputtering. *Modern Physics Letters B*, *23*, 3157-3170. https://doi.org/10.1142/S0217984909021211

Amalathas, A. P., & Alkaisi, M. M. (2016). Effects of film thickness and sputtering power on properties of ITO thin films deposited by RF magnetron sputtering without oxygen. *Journal of Materials Science: Materials in Electronics, 27*(10), 11064-1071. https://doi.org/10.1007/s10854-016-5223-9

Amrani, R., Garoudja, E., Lekoui, F., Filali, W., Neggaz, H., Djebeli, Y. A., Henni, L., Hassani, S., Kezzoula, F., Oussalah, S., Al mashary, F., & Henini, M. (2023). Investigation of structural and electrical properties of ITO thin films and correlation to optical parameters extracted using novel method based on PSO algorithm. *Bulletin of Materials Science*, *46*(1), Article 8. https://doi.org/10.1007/s12034-022-02845-8

Antony, A., Nisha, M., Manoj, R., & Jayaraj, M. K. (2004). Influence of target to substrate spacing on the properties of ITO thin films. *Applied Surface Science*, *225*(1-4), 294-301. https://doi.org/10.1016/j.apsusc.2003.10.017

Aperathitis, E., Bender, M., Cimalla, V., Ecke, G., & Modreanu, M. (2003). Properties of rf-sputtered indium-tin-oxynitride thin films. *Journal of Applied Physics*, *94*(2), 1258-1266. https://doi.org/10.1063/1.1582368

Atabaev, I. G., Khazhiev, M. U., Zakirova, S. B., & Shermatov, Z. (2017). Correlation between the structure, specific resistance, and optical properties of ITO films grown by CVD. *Applied Solar Energy (English Translation of Geliotekhnika)*, *53*(4), 322-325. https://doi.org/10.3103/S0003701X1704003X

Avelar-Muñoz, F., Berumen, J. A., Aguilar-Frutis, M. A., Araiza, J. J., & Ortega, J. J. (2020). Enhancement on carrier mobility in amorphous indium tin oxynitride (ITON) thin films. *Journal of Alloys and Compounds*, *835*, Article 155353. https://doi.org/10.1016/j.jallcom.2020.155353

Balasubramanian, N., & Subrahmanyam, A. (1989). Electrical and optical properties of reactively evaporated indium tin oxide (ITO) films-dependence on substrate temperature and tin concentration. *Journal of Physics D: Applied Physics*, *22*(1), 206-209. https://doi.org/10.1088/0022-3727/22/1/030

Biswas, N., Ghosh, P., Sarkar, S., Moitra, D., Biswas, P. K., Jana, S., & Mukhopadhyay, A. K. (2015). Nanomechanical properties of dip coated indium tin oxide films on glass. *Thin Solid Films*, *579*, 21-29. https://doi.org/10.1016/j.tsf.2015.02.030

Chen, P. H., Shih, H. J., & Li, P. J. (2019). Effects of varying nitride concentration in Ar:N_2 sputtering

of indium-tin-oxide film for use as electrode in resistance switching device. *Journal of Alloys and Compounds*, *808*, Article 151654. https://doi.org/10.1016/j.jallcom.2019.151654

Cho, S., & Kim, M. (2013). Effects of nitrogen flow rate on the properties of indium oxide thin films. *Journal of Nanoscience and Nanotechnology*, *13*(11), 7788-7792. https://doi.org/10.1166/jnn.2013.7811

Das, R., Adhikary, K., & Ray, S. (2007). The role of oxygen and hydrogen partial pressures on structural and optical properties of ITO films deposited by reactive rf-magnetron sputtering. *Applied Surface Science*, *253*(14), 6068-6073. https://doi.org/10.1016/j.apsusc.2007.01.107

Ellmer, K. (2012). Past achievements and future challenges in the development of optically transparent electrodes. *Nature Photonics*, *6*(12), 809-817. https://doi.org/10.1038/nphoton.2012.282

Eshaghi, A., & Graeli, A. (2014). Optical and electrical properties of indium tin oxide (ITO) nanostructured thin films deposited on polycarbonate substrates “thickness effect.” *Optik*, *125*(3), 1478-1481. https://doi.org/10.1016/j.ijleo.2013.09.011

Fallah, H. R., Ghasemi, M., Hassanzadeh, A., & Steki, H. (2007). The effect of annealing on structural, electrical and optical properties of nanostructured ITO films prepared by e-beam evaporation. *Materials Research Bulletin*, *42*(3), 487-496. https://doi.org/10.1016/j.materresbull.2006.06.024

Fan, J. C. C., & Goodenough, J. B. (1977). X-ray photoemission spectroscopy studies of Sn-doped indium-oxide films. *Journal of Applied Physics*, *48*(8), 3524-3531.

Fraser, D. B., & Cook, H. D. (1972). Highly Conductive, Transparent Films of Sputtered $In_{[2-x]}Sn_{[x]}O_{[3-y]}$. *Journal of The Electrochemical Society*, *119*(10), Article 1368. https://doi.org/10.1149/1.2403999

Gartner, M., Stroescu, H., Marin, A., Osiceanu, P., Anastasescu, M., Stoica, M., Nicolescu, M., Duta, M., Preda, S., Aperathitis, E., Pantazis, A., Kampylafka, V., Modreanu, M., & Zaharescu, M. (2014). Effect of nitrogen incorporation on the structural, optical and dielectric properties of reactive sputter grown ITO films. *Applied Surface Science*, *313*, 311-319. https://doi.org/10.1016/j.apsusc.2014.05.208

Gorjanc, T. C., Leong, D., Py, C., & Roth, D. (2002). Room temperature deposition of ITO using R.F. Magnetron sputtering. *Thin Solid Films*, *413*(1-2), 181-185. https://doi.org/10.1016/S0040-6090(02)00425-X

Granqvist, C. G. (2007). Transparent conductors as solar energy materials: A panoramic review. *Solar Energy Materials and Solar Cells*, *91*(17), 1529-1598. https://doi.org/10.1016/j.solmat.2007.04.031

Gupta, L., Mansingh, A., & Srivastava, P. K. (1989). Band gap narrowing and the band structure of tin-doped indium oxide films. *Thin Solid Films*, *176*(1), 33-44. https://doi.org/10.1016/0040-6090(89)90361-1

Hao, L., Diao, X., Xu, H., Gu, B., & Wang, T. (2008). Thickness dependence of structural, electrical and optical properties of indium tin oxide (ITO) films deposited on PET substrates. *Applied Surface Science*, *254*(11), 3504-3508. https://doi.org/10.1016/j.apsusc.2007.11.063

Hotovy, J., Hüpkes, J., Böttler, W., Marins, E., Spiess, L., Kups, T., Smirnov, V., Hotovy, I., & Kováč, J. (2013). Sputtered ITO for application in thin-film silicon solar cells: Relationship between structural and electrical properties. *Applied Surface Science*, *269*, 81-87. https://doi.org/10.1016/j.apsusc.2012.10.180

Hu, Y., Diao, X., Wang, C., Hao, W., & Wang, T. (2004). Effects of heat treatment on properties of ITO films prepared by rf magnetron sputtering. *Vacuum*, *75*(2), 183-188. https://doi.org/10.1016/j.vacuum.2004.01.081

Huang, T., Mo, C., Cui, M., Li, M., Ji, P., Tan, H., Zhang, X., Zhuge, L., & Wu, X. (2024). Ion behavior impact on ITO thin film fabrication via DC magnetron sputtering with external anode. *Vacuum*, *221*, Article 112848. https://doi.org/10.1016/j.vacuum.2023.112848

Hukari, K., Dannenberg, R., & Stach, E. A. (2002). Nitrogen effects crystallization kinetics

of amorphous TiO_xN_y thin films. *Journal of Materials Research*, *17*(3), 550-555. https://doi.org/10.1557/JMR.2002.0077

Jung, Y. S., & Lee, S. S. (2003). Development of indium tin oxide film texture during DC magnetron sputtering deposition. *Journal of Crystal Growth*, *259*(4), 343-351. https://doi.org/10.1016/j.jcrysgro.2003.07.006

Kim, J. H., Lee, J. H., Heo, Y. W., Kim, J. J., & Park, J. O. (2009). Effects of oxygen partial pressure on the preferential orientation and surface morphology of ITO films grown by RF magnetron sputtering. *Journal of Electroceramics*, *23*(2-4), 169-174. https://doi.org/10.1007/s10832-007-9351-8

Kim, J. H., Seong, T. Y., Ahn, K. J., Chung, K. B., Seok, H. J., Seo, H. J., & Kim, H. K. (2018). The effects of film thickness on the electrical, optical, and structural properties of cylindrical, rotating, magnetron-sputtered ITO films. *Applied Surface Science*, *440*, 1211-1218. https://doi.org/10.1016/j.apsusc.2018.01.318

Koseoglu, H., Turkoglu, F., Kurt, M., Yaman, M. D., Akca, F. G., Aygun, G., & Ozyuzer, L. (2015). Improvement of optical and electrical properties of ITO thin films by electro-annealing. *Vacuum*, *120*, 8-13. https://doi.org/10.1016/j.vacuum.2015.06.027

Kurdesau, F., Khripunov, G., da Cunha, A. F., Kaelin, M., & Tiwari, A. N. (2006). Comparative study of ITO layers deposited by DC and RF magnetron sputtering at room temperature. *Journal of Non-Crystalline Solids*, *352*(9-20), 1466-1470. https://doi.org/10.1016/j.jnoncrysol.2005.11.088

Lacroix, B., Paumier, F., Santos, A. J., Maudet, F., Girardeau, T., Dupeyrat, C., García, R., & Morales, F. M. (2022). Texture in ITO films deposited at oblique incidence by ion beam sputtering. *Applied Surface Science*, *605*, Article 154677. https://doi.org/10.1016/j.apsusc.2022.154677

Lai, A. R., Ali, A. H., Sani, N., & Azali, M. M. (2023). Characterization the optical band gap of indium tin oxide based on different thickness. *Enhanced Knowledge in Sciences and Technology*, *3*(1), 160-168.

Li, J., Jiang, L., Li, X., Luo, J., Liu, J., Wang, M., & Yan, Y. (2023). Different crystallization behavior of amorphous ITO film by rapid infrared annealing and conventional furnace annealing technology. *Materials*, *16*(10), Article 3803. https://doi.org/10.3390/ma16103803

Liu, Z., Liang, J., Zhou, H., Sun, H., Lu, W., Wang, B., Li, Q., Zhao, X., Wang, D., & Xu, J. (2023). Effect of nitrogen partial pressure on the piezoresistivity of magnetron sputtered ITO thin films at high temperatures. *Applied Surface Science, 608*, Article 155292. https://doi.org/10.1016/j.apsusc.2022.155292

Liu, Z., Liang, J., Li, J., Yang, M., Cao, S., & Xu, J. (2021). Effect of nitrogen-doped concentration on the TCR of ITO thin films at high temperature. In *2021 IEEE 34th international conference on micro electromechanical systems (MEMS)* (pp. 856-859). https://doi.org/10.1109/MEMS51782.2021.9375245

Markov, L. K., Pavluchenko, A. S., Smirnova, I. P., Aksenova, V. V, Yagovkina, M. A., & Klinkov, V. A. (2023). Formation of the structured indium tin oxide films by magnetron sputtering. *Thin Solid Films*, *774*, Article 139848. https://doi.org/10.1016/j.tsf.2023.139848

Mazur, M., Pastuszek, R., Wojcieszak, D., Kaczmarek, D., Domaradzki, J., Obstarczyk, A., & Lubanska, A. (2022). Effect of thickness on optoelectronic properties of ITO thin films. *Circuit World*, *48*(2), 149-159. https://doi.org/10.1108/CW-11-2019-0170

Minami, T., Kakumu, T., Shimokawa, K., & Takata, S. (1998). New transparent conducting ZnO-In_2O_3-SnO_2 thin films prepared by magnetron sputtering. *Thin Solid Films*, *317*(1-2), 318-321. https://doi.org/10.1016/S0040-6090(97)00547-6

Nguyen, T. T., Dao, K. A., Nguyen, T. T., Nguyen, C. D., Nguyen, S. H., & Nguyen, T. M. H. (2020). Influence of thermal annealing media on optical and electrical properties of FTO, ITO and TiO_2 films. *Materials Transactions*, *61*(11), 2091-2094.

https://doi.org/10.2320/matertrans.MT-MN2019002

Ni, J. H., Sarney, W. L., Leff, A. C., Cahill, J. P., & Zhou, W. (2020). Property variation in wavelength-thick epsilon-near-zero ITO metafilm for near IR photonic devices. *Scientific Reports*, *10*(1), Article 713. https://doi.org/10.1038/s41598-020-57556-z

Nuchuay, P., Chaikeeree, T., Horprathum, M., Mungkung, N., Kasayapanand, N., Oros, C., Limwichean, S., Nuntawong, N., Chananonnawathorn, C., Patthanasettakul, V., Muthitamongkol, P., Samransuksamer, B., Denchitcharoen, S., Klamchuen, A., Thanachayanont, C., & Eiamchai, P. (2017). Engineered omnidirectional antireflection ITO nanorod films with super hydrophobic surface via glancing-angle ion-assisted electron-beam evaporation deposition. *Current Applied Physics*, *17*(2), 222-229. https://doi.org/10.1016/j.cap.2016.11.018

Ollotu, E. R., Nyarige, J. S., Mlyuka, N. R., Samiji, M. E., & Diale, M. (2020). Properties of ITO thin films rapid thermally annealed in different exposures of nitrogen gas. *Journal of Materials Science: Materials in Electronics*, *31*, 16406-16413. https://doi.org/10.1007/s10854-020-04192-y

Phillips, J. M., Cava, R. J., Thomas, G. A., Carter, S. A., Kwo, J., Siegrist, T., Krajewski, J. J., Marshall, J. H., Peck, W. F., & Rapkine, D. H. (1995). Zinc-indium-oxide: A high conductivity transparent conducting oxide. *Applied Physics Letters*, *67*(15), 2246-2248. https://doi.org/10.1063/1.115118

Pokaipisit, A., Horprathum, M., & Limsuwan, P. (2007). Effect of films thickness on the properties of ITO thin films prepared by electron beam evaporation. *Kasetsart Journal (Natural Science)*, *41*, 255-261.

Pokaipisit, A., Horprathum, M., & Limsuwan, P. (2008). Influence of annealing temperature on the properties of ITO films prepared by electron beam evaporation and ion-assisted deposition. *Nature Science*, *42*(5), 362-366.

Polychronopoulou, K., Baker, M. A., Rebholz, C., Neidhardt, J., O'Sullivan, M., Reiter, A. E., Kanakis, K., Leyland, A., Matthews, A., & Mitterer, C. (2009). The nanostructure, wear and corrosion performance of arc-evaporated CrB_xN_y nanocomposite coatings. *Surface and Coatings Technology*, *204*(3), 246-255. https://doi.org/10.1016/j.surfcoat.2009.07.009

Polychronopoulou, K., Rebholz, C., Baker, M. A., Theodorou, L., Demas, N. G., Hinder, S. J., Polycarpou, A. A., Doumanidis, C. C., & Böbel, K. (2008). Nanostructure, mechanical and tribological properties of reactive magnetron sputtered TiC_x coatings. *Diamond and Related Materials*, *17*(12), 2054-2061. https://doi.org/10.1016/j.diamond.2008.07.007

Qiao, Z., & Mergel, D. (2005). Comparison of radio-frequency and direct-current magnetron sputtered thin In_2O_3: Sn films. *Thin Solid Films*, *484*(1-2), 146-153. https://doi.org/10.1016/j.tsf.2005.02.006

Rebholz, C., Monclus, M. A., Baker, M. A., Mayrhofer, P. H., Gibson, P. N., Leyland, A., & Matthews, A. (2007). Hard and superhard TiAlBN coatings deposited by twin electron-beam evaporation. *Surface and Coatings Technology*, *201*(13), 6078-6083. https://doi.org/10.1016/j.surfcoat.2006.08.121

Robb, A. J., Duca, Z. A., White, N., Woodell, P., & Ward, P. A. (2024). Influence of oxygen on the optical and electrical properties of magnetron-sputtered indium tin oxide thin films at ambient temperature. *Thin Solid Films*, *788*, Article 140152. https://doi.org/10.1016/j.tsf.2023.140152

Shigesato, Y., Paine, D. C., & Haynes, T. E. (1993). Study of the effect of ion implantation on the electrical and microstructural properties of tin-doped indium oxide thin films. *Journal of Applied Physics*, *73*(8), 3805-3811. https://doi.org/10.1063/1.352887

Sparvoli, M., Mansano, R. D., & Chubaci, J. F. D. (2013). Study of indium nitride and indium oxynitride band gaps. *Materials Research*, *16*(4), 850-852. https://doi.org/10.1590/S1516-14392013005000063

Tchenka, A., Agdad, A., Vall, M. C. S., Hnawi, S. K., Narjis, A., Nkhaili, L., Ibnouelghazi, E., & Ech-Chamikh, E. (2021). Effect of RF sputtering power and deposition time on optical and electrical properties of indium tin oxide thin film. *Advances in Materials Science and Engineering*, *2021*, Article 5556305. https://doi.org/10.1155/2021/5556305

Thakur, J. S., Danylyuk, Y. V., Haddad, D., Naik, V. M., Naik, R., & Auner, G. W. (2007). Influence of defects on the absorption edge of InN thin films: The band gap value. *Physical Review B - Condensed Matter and Materials Physics*, *76*(3), Article 035309. https://doi.org/10.1103/PhysRevB.76.035309

Wang, Y., Bruyère, S., Kumagai, Y., Tsunoda, N., Oba, F., Ghanbaja, J., Sun, H., Dai, B., & Pierson, J. F. (2022). Tuning the optical band gap and electrical properties of NiO thin films by nitrogen doping: a joint experimental and theoretical study. *RSC Advances*, *12*(34), 21940-21945. https://doi.org/10.1039/d2ra01887j

Wang, Y., & Tang, W. (2017). Surface-dependent conductivity, transition type, and energy band structure in amorphous indium tin oxide films. *Solid-State Electronics*, *138*, 79-83. https://doi.org/10.1016/j.sse.2017.09.007

Yang, S., Zhang, C., Yang, Z., Yao, J., Wang, H., & Ding, G. (2019). Effect of nitrogen doping temperature on the resistance stability of ITO thin films. *Journal of Alloys and Compounds*, *784*, 1234-1242. https://doi.org/10.1016/j.jallcom.2018.11.126

Yang, S., Sun, B., Liu, Y., Zhu, J., Song, J., Hao, Z., Zeng, X., Zhao, X., Shu, Y., Chen, J., Yi, J., & He, J. (2020). Effect of ITO target crystallinity on the properties of sputtering deposited ITO films. *Ceramics International*, *46*(5), 6342-6350. https://doi.org/10.1016/j.ceramint.2019.11.110

Zhang, L., Lan, J., Yang, J., Guo, S., Peng, J., Zhang, L., Tian, S., Ju, S., & Xie, W. (2017). Study on the physical properties of indium tin oxide thin films deposited by microwave-assisted spray pyrolysis. *Journal of Alloys and Compounds*, *728*, 1338-1345. https://doi.org/10.1016/j.jallcom.2017.09.024

Zubair, M. A., Chowdhury, M. T., Bashar, M. S., Sami, M. A., & Islam, M. F. (2019). Thickness dependent correlation between structural and optical properties of textured CdSe thin film. *AIP Advances*, *9*(4), Article 045123. https://doi.org/10.1063/1.5096594